ADVANCED ENERGY MATERIALS
www.advenergymat.de

Ternary Organic Solar Cells With 12.8% Efficiency Using Two Nonfullerene Acceptors With Complementary Absorptions

Bin Kan, Yuan-Qiu-Qiang Yi, Xiangjian Wan, Huanran Feng, Xin Ke, Yanbo Wang, Chenxi Li, and Yongsheng Chen**

A new small-molecule acceptor (2,9-bis(2-methylene-(3(1,1-dicyanomethylene) benz[f]indanone))7,12-dihydro-(4,4,10,10-tetrakis(4-hexylphenyl)-5,11-diocthylthieno[3′,2′:4,5]cyclopenta[1,2-b]thieno[2″,3″:3′,4′]cyclopenta[1′,2′:4,5]thieno[2,3-f][1]benzothiophene) (NNBDT) based on naphthyl-fused indanone ending units is reported. This molecule shows a narrow optical bandgap of 1.43 eV and effective absorption in the range of 700–870 nm. The devices based on poly[(2,6-(4,8-bis(5-(2-ethylhexyl)thiophen-2-yl)-benzo[1,2-b:4,5-b′]dithiophene))-alt-(5,5-(1′,3′-di-2-thienyl-5′,7′-bis(2-ethylhexyl)benzo[1′,2′-c:4′,5′-c′]dithiophene-4,8-dione))] (PBDB-T):NNBDT yield a power conversion efficiency of 11.7% with a low energy loss of 0.55 eV and a high fill factor (FF) of 71.7%. Another acceptor (2,9-bis(2-methylene-(3(1,1-dicyanomethylene)benz[f]indanone))7,12-dihydro-4,4,7,7,12,12-hexaoctyl-4*H*-cyclopenta[2″,1″:5,6;3″,4″:5′,6′]diindeno[1,2-b:1′,2′-b′]dithiophene (FDNCTF) is introduced as the third component to fabricate ternary devices. The two acceptors (NNBDT and FDNCTF) possess complementary absorption, same molecular orientation, and well-miscible behavior. It is found that there exists a nonradiative energy transfer process from FDNCTF to NNBDT. The fullerene-free ternary cells based on PBDB-T:NNBDT:FDNCTF achieve a high efficiency of 12.8% with an improved short circuit current near 20 mA cm^{-2} in contrast to the binary devices. The result represents the best performance for fullerene-free ternary solar cells reported to date and highlights the potential of ternary solar cells.

Solution-processed organic solar cells (OSCs), as an alternative green technology to utilize solar energy, have drawn extensive attentions due to their potential in the flexible electronic devices.[1–3] Due to the rapid evolution of novel nonfullerene acceptors (NFAs) and wide-bandgap polymer donors,[4–12] the fullerene free–based devices with bulk heterojunction architecture have achieved impressive enhancement with power conversion efficiencies (PCEs) up to 13%.[13–15] Small-molecule acceptors (SMAs) with acceptor–donor–acceptor (A–D–A) structure, which possess defined chemical structures, finely tuned energy levels, and strong absorption ability, play a vital role in the development of NF-OSCs.[16–21] In 2015, Zhan and co-workers reported an A–D–A-type SMA (known as ITIC) based on a ladder-type core unit with an initial performance of 6.8%.[22] By altering the chemical structures of ladder-type unit (D) and/or ending groups (A), a variety of SMAs with high performance have been explored.[16,23–28] Besides the versatility of ladder-type core units, modifying the common ending unit 2-(2,3-dihydro-3-oxo-1*H*-inden-1-ylidene)propanedinitrile (INCN), such as methyl, methoxy, and halogen substitutions, is a feasible method toward designing novel SMAs.[13,27,29,30] Recently, we successfully exploited a novel naphthyl-fused indanone (NINCN) end groups with the extended conjugation to manage the balance of short circuit current (J_{sc}) and open circuit voltage (V_{oc}).[31] Compared to 2,9-bis(2-methylene(3(1,1dicyanomethylene)-indanone))7,12-dihydro-4,4,7,7,12,12-hexaoctyl-4*H*-cyclopenta[2″,1″:5,6;3″,4″:5′,6′]diindeno[1,2-b:1′,2′-b′]dithiophene (FDICTF) with the INCN units,[17] (2,9-bis(2-methylene-(3(1,1-dicyanomethylene)benz[f]indanone))7,12-dihydro-4,4,7,7,12,12-hexaoctyl-4*H*-cyclopenta[2″,1″:5,6;3″,4″:5′,6′]diindeno[1,2-b:1′,2′-b′]dithiophene (FDNCTF) with the NINCN units exhibited enhanced molecular interaction, red-shifted optical absorption, and more ordered packing at solid state, leading to better OSC performance. Afterward, Hou and co-workers reported a new SMA with the same ending unit and achieved a remarkable fill factor (FF) of 0.78.[32] These results strengthen the idea that the NINCN unit has great potential for designing high-performance SMAs.

Meanwhile, device optimizations including solvent additives, post-treatment, and interfacial layer materials are of great significance in improving the performance of OSCs.[33–35] Among different strategies, ternary OSCs (two donors and one

B. Kan, Y.-Q.-Q. Yi, Prof. X. Wan, H. Feng, X. Ke, Y. Wang, Prof. C. Li, Prof. Y. Chen
State Key Laboratory and Institute of Elemento-Organic Chemistry
The Centre of Nanoscale Science and Technology and Key Laboratory of Functional Polymer Materials
College of Chemistry
Nankai University
Tianjin 300071, China
E-mail: xjwan@nankai.edu.cn; yschen99@nankai.edu.cn
The ORCID identification number(s) for the author(s) of this article can be found under https://doi.org/10.1002/aenm.201800424.

DOI: 10.1002/aenm.201800424

acceptor, or one donor and two acceptors) can effectively cover wide absorption range and utilize more photons, which are beneficial for obtaining high J_{sc}.[36–43] Additionally, the V_{oc} of the host binary devices can be maintained by selecting the third component that has similar voltage output.[41,44] It is believed that ternary OSCs containing one donor and two NF-SMAs have great potentials in reducing energy loss, enhancing light absorption strength, and achieving high performance.[45,46] For example, Sun and co-workers first demonstrated over 10% efficiency ternary cells containing two nonfullerene acceptors SdiPDBI-Se and ITIC-Th with complementary absorption in the visible range.[47] Hou and co-workers fabricated ternary fullerene-free OSCs with performance of 11.1% based on polymer donor J52 and two SMAs (IT-M and IEICO).[48] Those two acceptors exhibited similar chemical structures and excellent molecular compatibility, which may worked as "one acceptor" in the ternary blending films. Together with their complementary absorption and similar lowest unoccupied molecular orbitals (LUMO) levels, the strategy using two well-miscible SMAs could simplify the ternary device optimization procedure and offer high performance simultaneously. Recently, PCEs exceeding 12% have been achieved by searching a suitable SMA as the third component for the primary binary blends, which highlight the promising future of fullerene-free ternary cells.[49]

In this study, we designed and synthesized a new A–D–A type SMA, named NNBDT (shown in **Figure 1**a), using NINCN as ending groups and a highly planar unit (4,4,10,10-tetrakis(4-hexylphenyl)-4,10-dihydro-5,11-diocthylthieno[3′,2′:4,5]cyclopenta[1,2-b]thieno[2″,3″:3′,4′]cyclopenta[1′,2′:4,5]thieno[2,3-f][1]benzothiophene) (CBDT) as the core block. NNBDT exhibits a low optical bandgap (E_g^{opt}) of 1.43 eV with an effective absorption range of 700–870 nm. When blended with wide bandgap polymer poly[(2,6-(4,8-bis(5-(2-ethylhexyl)thiophen-2-yl)-benzo[1,2-b:4,5-b′]dithiophene))-alt-(5,5-(1′,3′-di-2-thienyl-5′,7′-bis(2-ethylhexyl)benzo[1′,2′-c:4′,5′-c′]dithiophene-4,8-dione))] (PBDB-T), a high PCE of 11.7% with a V_{oc} of 0.88 V could be achieved for the PBDB-T:NNBDT-based devices. The energy loss is as low as 0.55 eV. The FDNCTF is selected as the third component to fabricate ternary solar cells due to its effective absorption in the range of 650–750 nm, suitable energy levels and similar chemical structure to NNBDT. Impressively, the ternary devices based on PBDB-T:NNBDT:FDNCTF exhibit a V_{oc} of 0.887 V, an enhanced J_{sc} of 19.89 mA cm^{-2} and FF of 72.2%. All these allow the optimized ternary device to reach the maximum PCE of 12.8%, which is the best performance for fullerene-free ternary OSCs to date.

The synthetic procedures and characterization data of NNBDT can be found in the Supporting Information. The NINCN unit and dialdehyde compound 4,4,10,10-tetrakis(4-hexylphenyl)-4,10-dihydro-5,11-diocthylthieno[3′,2′:4,5]cyclopenta[1,2-b]thieno[2″,3″:3′,4′]cyclopenta[1′,2′:4,5]thieno[2,3-f][1]benzothiophene-2,8-dicarboxaldehyde (DFCBDT) were prepared as our reported methods.[20,31] The target molecule NNBDT was then synthesized by the Knoevenagel condensation with these two compounds in high yield. NNBDT exhibited a decomposition temperature (T_d) of 350 °C with 5% weight loss determined from thermogravimetric analysis (TGA) curves (Figure S1, Supporting Information), indicating its good thermal stability. It is worth noting that the chemical structures of NNBDT and FDNCTF are quite similar since they are both based on the NINCN ending groups and heptacyclic fused-ring core with six side chains. The six side chains of NNBDT not only enable its good solubility in common organic solvents (such as chloroform and chlorobenzene) but also can effectively avoid strong aggregation in the solid state. To evaluate the miscible behavior between NNBDT and FDNCTF in solid state, the morphologies of NNBDT

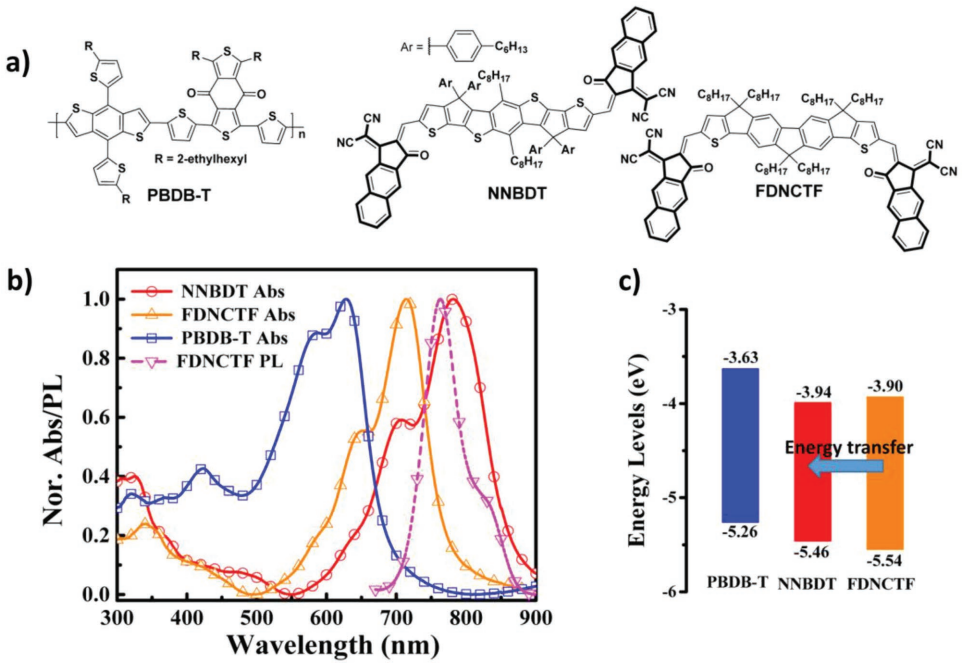

Figure 1. a) Chemical structures of PBDB-T, NNBDT, and FDNCTF. b) Normalized thin-film absorption spectra of PBDB-T, NNBDT, and FDNCTF. PL spectrum of FNDCTF (dot line). c) The energy diagrams of PBDB-T, NNBDT, and FDNCTF.

pristine film and NNBDT:FDNCTF blend film were investigated by the atomic force microscopy (AFM) shown as Figure S2 in the Supporting Information. It can be seen that both films were smooth with low roughness. There was no obvious molecular over-aggregation or isolated domains in the NNBDT:FDNCTF film, suggesting good compatibility between these rather similar acceptors as further evidenced by grazing-incidence wide-angle X-ray scattering (GIXD) results discussed below.

As seen from Figure S3 in the Supporting Information, the UV–vis spectrum of NNBDT in diluted $CHCl_3$ solution displays an absorption peak at 752 nm with a maximum absorption coefficient of 2.4×10^5 M^{-1} cm^{-1}. The normalized thin-film absorption spectra of NNBDT, FDNCTF, and PBDB-T are summarized in Figure 1b. PBDB-T, FDNCTF, and NNBDT in thin-films exhibit distinct absorption peaks located at 628, 713, and 782 nm, respectively, implying a complementary absorption ranging from the visible light to the near-infrared region (NIR). The E_g^{opt} of NNBDT, calculated from its absorption onset of 866 nm, is as low as 1.43 eV. Compared to the PBDB-T:NNBDT film, the optimal ternary film yields enhanced absorption ability in the range of 650–750 nm shown in Figure S4 in the Supporting Information, which are beneficial for utilizing more solar photons in their absorption spectra region.[50] The energy levels of these two acceptors as well as PBDB-T were measured in the thin-film state by cyclic voltammetry methods (Figure S5, Supporting Information). Their highest occupied molecular orbitals (HOMOs) and LUMOs energy levels could be calculated from their onset oxidation and reduction potentials, respectively. As depicted in Figure 1c, the HOMO and LUMO levels of NNBDT are −5.46 and −3.94 eV, respectively. FDNCTF exhibits a LUMO level of −3.90 eV between the LUMO of PBDB-T and NNBDT, which can produce a higher V_{oc} as well as facilitate charge transport from donor to the acceptors.

Figure 1b shows that the photoluminescence (PL) spectrum of FDNCTF is totally covered by the absorption spectrum of NNBDT, and this is a spectral indication of a possible nonradiative energy transfer process from FDNCTF to NNBDT.[37,48] To verify this, the PL emission spectra of FDNCTF:NNBDT (8:2) film together with those of NNBDT and FDNCTF pristine films were measured at the excitation wavelength of 670 nm. As depicted in Figure S6 in the Supporting Information, the NNBDT:FDNCTF blend film delivered the same emission peak at ≈832 nm as NNBDT pristine film. Importantly, the PL intensity of blend film was nearly two times than that of NNBDT pristine film, and the PL intensity of FDNCTF fully disappeared in the blend. These results indicate that there is an efficient energy transfer process from FDNCTF to NNBDT. Therefore, another possible channel to generate charges of FDNCTF excitons can be formed via such an energy transfer to NNBDT and then hole to PBDB-T, which is different from the pathway directly existed at the PBDB-T:FDNCTF interfaces. When blended with donor PBDB-T, the PL intensity of PBDB-T (excited at 600 nm) and acceptors (excited at 670 nm) are quenched with high efficiencies, indicating the effective charge generation between PBDB-T and acceptors.

To evaluate the photovoltaic properties of NNBDT, solution-processed OSCs were fabricated with the conventional configuration of indium tin oxides (ITO)/poly(3,4-ethylenedioxythiopene): poly(styrenesulfonate) (PEDOT:PSS)/PBDB-T:acceptors/perylene diimide functionalized with amino N-oxide (PDINO)/Al, where PDINO was selected as electron transport layer due to its suitable energy levels and electron extraction ability.[51] After systematic device optimization (Tables S1–S3, Supporting Information), chloroform was used as the host solvent, the D:A ratio of binary device was optimized to be 1:0.8 and a tiny amount of 1,8-diiodooctane (DIO, 0.5% volume) was selected as solvent additive to tune the morphology. As a result, the PBDB-T:NNBDT device achieved a V_{oc} of 0.88 V and an FF of 71.7%. The energy loss (E_{loss}), defined as $E_{loss} = E_g^{opt} - eV_{oc}$ (where E_g^{opt} is refer to the optical bandgap of NNBDT), is only 0.55 eV. While, the moderate J_{sc} value of 18.63 mA cm^{-2} limits the overall device performance to 11.7%. In order to pursue a better performance and keep its high V_{oc}/low E_{loss} and FF, a quite similar acceptor FDNCTF was used as third component in PBDB-T:NNBDT to construct ternary cells. First, the performance of PBDB-T:FDNCTF-based device using chloroform (CF) as the host solvent was investigated. The corresponding device offered an exciting PCE of 10.8% with a V_{oc} of 0.909 V and an outstanding FF near 75%, which is comparable to our reported data.[31] Herein, we directly added molecule FDNCTF in the optimal PBDB-T:NNBDT blend film to fully exploit the advantages of the binary system, such as its low E_{loss}, strong and efficient absorption in the NIR. Consequently, a high PCE of 12.8% with a V_{oc} of 0.887 V, an enhanced J_{sc} near 20 mA cm^{-2} and almost the same FF could be achieved for PBDB-T:NNBDT:FDNCTF-based ternary devices at the ratio of 1:0.8:0.2 (Table S4, Supporting Information). The slightly enhanced V_{oc} could be ascribed to the contribution of FDNCTF.[43] To the best of our knowledge, this impressive PCE of 12.8% with E_{loss} below 0.60 eV is the best result for fullerene-free ternary OSCs. The performance histogram of the counts for binary devices and ternary devices are presented as Figure S7 in the Supporting Information. The current density–voltage (J–V) curves of the optimal binary and ternary device are shown as **Figure 2**b, and their corresponding parameters are summarized in **Table 1**. The stability of unencapsulated binary and ternary devices was tested for over 250 h in N_2 glove box (Figure S8, Supporting Information). At the starting age (≈48 h), the ternary and binary devices show similar degradation trend. And then the ternary device keeps almost stable with 92% of original value, higher than that (87%) of the binary device, which indicates better stability of ternary device.

Figure 2c shows the external quantum efficiency (EQE) curves for the binary and ternary devices. The NNBDT-based binary device showed wide photocurrent responses extending to ≈870 nm owing to the contribution of the low bandgap acceptor. High EQE values around 70% in the range of 500–630 and 690–780 nm could be observed, suggesting efficient charge transfer between polymer donor (PBDB-T) and acceptor (NNBDT). As depicted in Figure 2c, the mixing of FDNCTF in the binary device has little impact on the photocurrent responses range. In addition, the optimal ternary device achieved a higher maximum EQE value of 76% and over 70% in the range of 500–760 nm, which indicates more efficient photoelectron conversion process in the ternary device. These EQE results are well consistent with their absorption abilities for the corresponding blend films (Figure S4, Supporting Information). The integrated current densities for the PBDB-T:NNBDT and ternary devices are 18.43 and 19.46 mA cm^{-2}, respectively, which are both close to the J_{sc} values obtained from the J–V curves.

The charge generation and recombination behavior in the PBDB-T:NNBDT device and ternary device were then studied

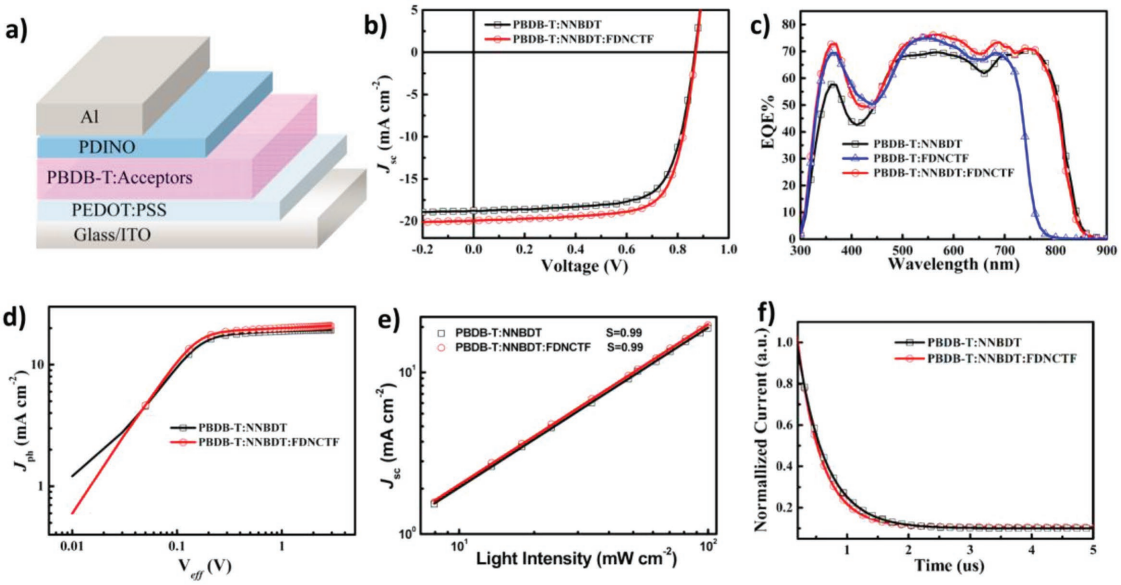

Figure 2. a) The diagram of conventional device structure. b) Current density–voltage (*J*–V) curve and c) EQE spectra of the PBDB-T:NNBDT device and ternary device. d) J_{ph} versus V_{eff} and e) light-intensity dependence of J_{sc} and f) TPC of PBDB-T:NNBDT and ternary devices, respectively.

according to the reported methods.[52,53] Figure 2d shows the photocurrent (J_{ph}) versus the effective applied voltage (V_{eff}) for the corresponding devices. When V_{eff} exceeds 1.5 V, J_{ph} for both devices reached saturation (J_{sat}), suggesting minimal charge recombination at high voltages.[51] The overall charge dissociation probability, estimated from the ratio of J_{ph}/J_{sat} under the short circuit conditions, was almost the same for the PBDB-T:NNBDT-based device and the ternary device (96.3% vs 96.1%). Compared to the binary device, the ternary device achieved a higher J_{sat}, which is an indicative of enhanced exciton generation rate. Besides, slopes near unit from the light-intensity dependence of J_{sc} results (Figure 2e) were observed for both optimal devices, which suggest quite similar but negligible bimolecular recombination, supporting their both high FFs.[54] The charge transport properties in the PBDB-T:NNBDT and ternary blend films were measured by space-charge-limited current (SCLC) using the electron-only and hole-only devices, respectively. The calculated electron and hole mobilities for PBDB-T:NNBDT-based devices are 7.57×10^{-5} and 1.78×10^{-4} cm^{-2} V^{-1} s^{-1}, respectively. After adding molecule FDNCTF, the ternary blend achieved higher electron (1.07×10^{-4} cm^{-2} V^{-1} s^{-1}) and hole (2.43×10^{-4} cm^{-2} V^{-1} s^{-1}) mobilities simultaneously. Furthermore, as evidenced from their transient photocurrent measurement results (Figure 2f), the optimized ternary device demonstrated a slightly shorter charge extraction time of 0.36 µs than that of the PBDB-T:NNBDT binary device (0.44 µs). All these factors contribute to improve the J_{sc} and keep the high FF for the ternary device, allowing for its high performance.[54,55]

The morphological differences between the PBDB-T:NNBDT film and the optimized ternary blend film were characterized by AFM and transmission electron microscopy (TEM) as shown in **Figure 3**. The PBDB-T:NNBDT film was featured with grain-like domains and exhibited a root-mean-square surface roughness (R_q) value of 1.95 nm. No large phase separation was observed from its TEM image. After adding FDNCTF, the ternary film gave a larger R_q value of 3.17 nm, which indicates more ordered nanoscale morphology in the blend. Meanwhile, the AFM and TEM images of ternary film shown growing and more continuous grain-like domains with proper size. The distinctive morphologies for the ternary film are more favorable for charge transport and collection in support of the aforementioned results.[35]

The molecular packing motifs and microstructure of NNBDT and FDNCTF pristine films were investigated by 2D-GIXD method, and their diffraction patterns with line-cut profiles were displayed as Figure S9 in the Supporting Information. The NNBDT film exhibited a lamellar diffraction peak (100) along its in-plane (IP) direction and a π–π stacking diffraction peak (010) along the out-of-plane (OOP) direction, which imply that

Table 1. Optimal device parameters of the binary and ternary devices under the illumination of AM 1.5G (100 mW cm^{-2}) using the conventional device structure.

BHJ layer	V_{oc} [V]	J_{sc} [mA cm^{-2}]	FF [%]	PCE [%]	E_{loss} [a)] [eV]
PBDB-T:NNBDT	0.880 (0.876 ± 0.003)[b)]	18.63 (18.44 ± 0.14)	71.7 (70.7 ± 0.6)	11.7 (11.5 ± 0.1)	0.55
PBDB-T:NNBDT:FDNCTF	0.887 (0.882 ± 0.003)	19.89 (19.68 ± 0.20)	72.2 (71.6 ± 0.5)	12.8 (12.5 ± 0.2)	0.54
PBDB-T:FDNCTF	0.909 (0.904 ± 0.005)	15.90 (15.60 ± 0.25)	74.6 (74.2 ± 0.3)	10.8 (10.6 ± 0.2)	0.69

[a)] $E_{loss} = E_g^{opt} - eV_{oc}$; [b)] The average values with standard deviations obtained from 20 devices are provided in the parentheses.

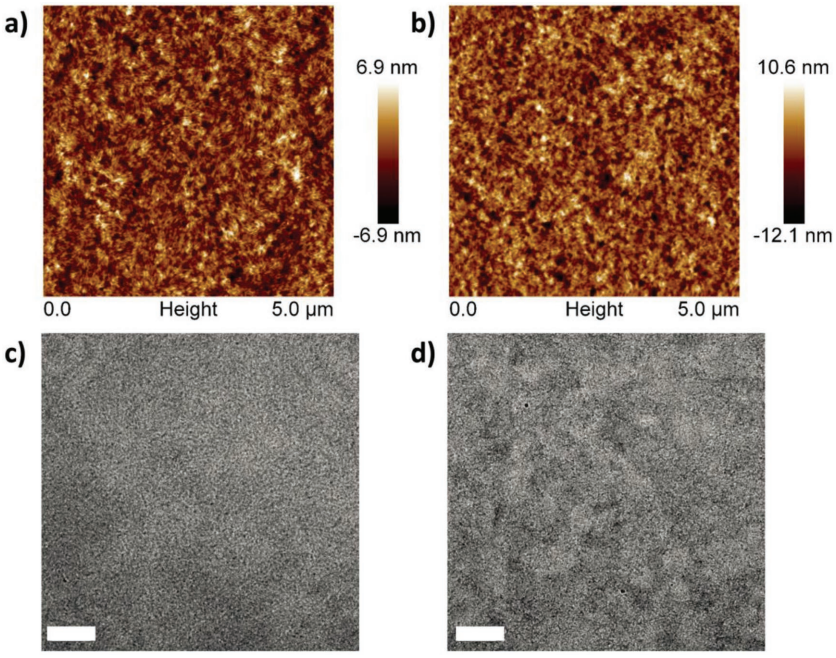

Figure 3. AFM and TEM images for a,c) PBDB-T:NNBDT film and b,d) PBDB-T:NNBDT:FDNCTF film. The scale bar are 200 nm.

NNBDT tends to form the face-on molecular orientation relative to substrate.[56] The (100) and (010) peaks for NNBDT were located at 0.29 and 1.82 $Å^{-1}$, corresponding to an alkyl-to-alkyl distance of 21.6 Å and a π–π stacking distance of 3.45 Å, respectively. The crystal coherence lengths (CCL) for NNBDT in the (100) and (010) directions, calculated by Scherrer equation,[57] were 9.7 and 2.9 nm, respectively. FDNCTF adopted the same face-on molecular packing as seen from Figure S9 in the Supporting Information. The CCLs for FDNCTF in the (100) and (010) directions were 20.9 and 3.8 nm, both larger than those of NNBDT, which suggest the better crystallinity of FDNCTF. As shown in Figure S10 in the Supporting Information, the optimized chemical structure of FDNCTF has better coplanar backbone and more ordered distribution of side chains than those of NNBDT, resulting in the better crystalline nature of FDNCTF. The GIXD patterns for the binary and ternary blend films and their in-plane line cuts were shown in **Figure 4**. Both binary films displayed broad

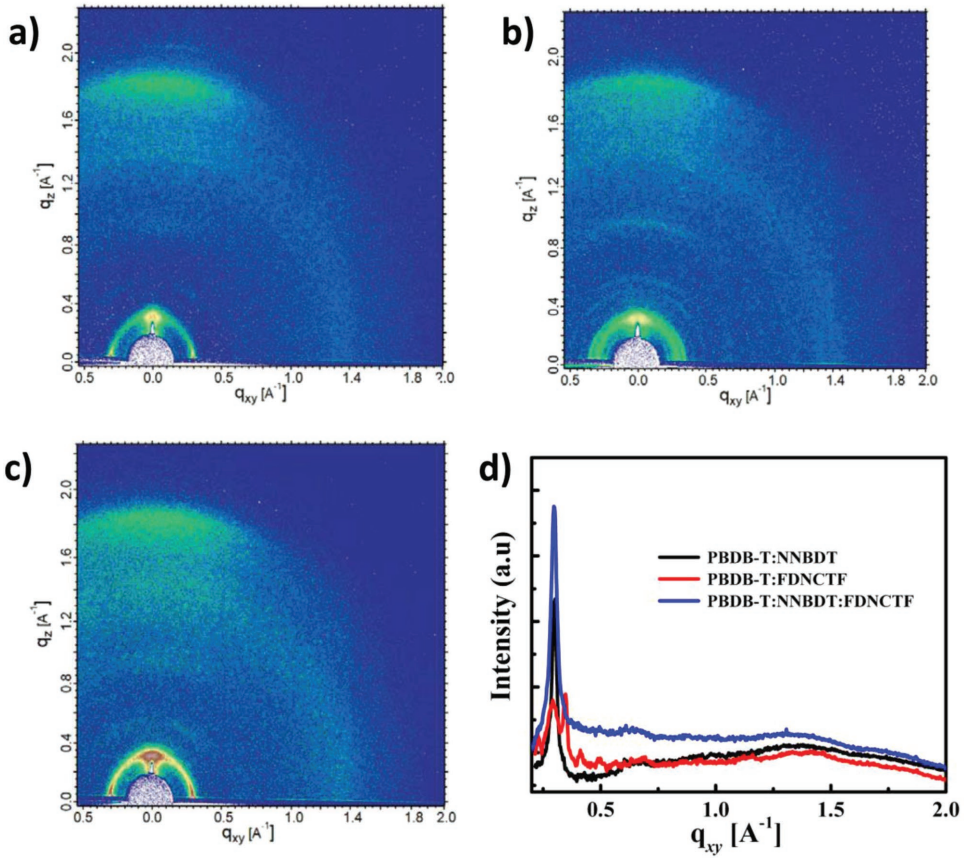

Figure 4. 2D-GIXD pattern for a) PBDB-T:NNBDT blend, b) PBDB-T:FDNCTF blend, and c) PBDB-T:NNBDT:FDNCTF blend films. d) In-plane line cuts of the corresponding GIXD patterns.

and combined diffraction peak in their (010) regions along the OOP direction, indicative of a preferred face-on orientation for PBDB-T, NNBDT, and FDNCTF in the films. Compared to PBDB-T:NNBDT film, the ternary film exhibited a similar diffraction pattern with enhanced intensities owing to more ordered molecular packing in the film as proved from the AFM results. Besides, as seen from Figure 4b and their in-plane line cuts, the PBDB-T:FDNCTF film gave two separated (100) diffraction peaks at 0.29 and 0.32 $Å^{-1}$, correlating to PBDB-T and FDNCTF, respectively. While, the ternary film still shown an emerged (100) diffraction peak at ≈0.30 $Å^{-1}$, which is the same as that of PBDB-T:NNBDT film. All these results mean that molecule FDNCTF not only did not sabotage the molecular packing orientations in the host binary but also could be well-miscible with NNBDT, which derived from its similar chemical structure and the same face-on orientation. Furthermore, the better crystallinity nature of FDNCTF leads more order molecular packing in the ternary film, which should be beneficial for charge transport, supporting the SCLC results.[58,59]

In conclusion, we designed and synthesized a narrow optical bandgap acceptor NNBDT using NINCN end groups. The device based on PBDB-T:NNBDT exhibited a PCE of 11.7% with a high FF of 71.7% and low energy loss of 0.55 eV. The device performance was further improved by introducing a third component FDNCTF, which has a similar chemical structure and good molecular compatibility with NNBDT. The ternary device based on PBDB-T:NNBDT:FDNCTF realized a high PCE of 12.8% with an enhanced J_{sc} near 20 mA cm^{-2} and almost unchanged V_{oc} and FF values. As far as we know, this result represents the best performance for all fullerene-free ternary OSCs reported to date. The improved overall performance could be attributed to the enhanced absorption ability and better charge transport properties in ternary blend film. Our work advances the idea that high performance ternary OSCs could be realized by using two similar NF-SMAs with suitable energy levels, complementary absorption, and same molecular orientations.

Supporting Information

Supporting Information is available from the Wiley Online Library or from the author.

Acknowledgements

The authors gratefully acknowledge the financial support from NSFC (91633301 and 51773095), MoST (2014CB643502) of China, Tianjin city (17JCJQJC44500, 17CZDJC31100), and 111 Project (B12015). The authors also thank beamline BL14B1 (Shanghai Synchrotron Radiation Facility) for providing the beam time.

Conflict of Interest

The authors declare no conflict of interest.

Keywords

high performance, nonfullerene acceptors, small molecules, ternary devices

Received: February 6, 2018
Revised: March 27, 2018
Published online:

[1] J. Y. Kim, K. Lee, N. E. Coates, D. Moses, T.-Q. Nguyen, M. Dante, A. J. Heeger, *Science* **2007**, *317*, 222.
[2] G. Li, R. Zhu, Y. Yang, *Nat. Photonics* **2012**, *6*, 153.
[3] L. Dou, Y. Liu, Z. Hong, G. Li, Y. Yang, *Chem. Rev.* **2015**, *115*, 12633.
[4] S. M. McAfee, J. M. Topple, I. G. Hill, G. C. Welch, *J. Mater. Chem. A* **2015**, *3*, 16393.
[5] C. B. Nielsen, S. Holliday, H. Y. Chen, S. J. Cryer, I. McCulloch, *Acc. Chem. Res.* **2015**, *48*, 2803.
[6] H. Bin, L. Gao, Z.-G. Zhang, Y. Yang, Y. Zhang, C. Zhang, S. Chen, L. Xue, C. Yang, M. Xiao, Y. Li, *Nat. Commun.* **2016**, *7*, 13651.
[7] J. Liu, S. Chen, D. Qian, B. Gautam, G. Yang, J. Zhao, J. Bergqvist, F. Zhang, W. Ma, H. Ade, H. Yan, *Nat. Energy* **2016**, *1*, 16089.
[8] S. Xiao, Q. Zhang, W. You, *Adv. Mater.* **2017**, *29*, 1601391.
[9] W. Zhao, S. Zhang, J. Hou, *Sci. China: Chem.* **2016**, *59*, 1574.
[10] H. Bin, L. Zhong, Z.-G. Zhang, L. Gao, Y. Yang, L. Xue, J. Zhang, Z. Zhang, Y. Li, *Sci. China: Chem.* **2016**, *59*, 1317.
[11] S. Li, W. Liu, C. Z. Li, M. Shi, H. Chen, *Small* **2017**, *13*, 1701120.
[12] Y. H. Cai, L. J. Huo, Y. M. Sun, *Adv. Mater.* **2017**, *29*, 1605437.
[13] W. Zhao, S. Li, H. Yao, S. Zhang, Y. Zhang, B. Yang, J. Hou, *J. Am. Chem. Soc.* **2017**, *139*, 7148.
[14] Z. Fei, F. D. Eisner, X. Jiao, M. Azzouzi, J. A. Rohr, Y. Han, M. Shahid, A. S. R. Chesman, C. D. Easton, C. R. McNeill, T. D. Anthopoulos, J. Nelson, M. Heeney, *Adv. Mater.* **2018**, *30*, 1705209.
[15] W. Zhao, S. Zhang, Y. Zhang, S. Li, X. Liu, C. He, Z. Zheng, J. Hou, *Adv. Mater.* **2018**, *30*, 1704837.
[16] Y. Lin, X. Zhan, *Adv. Energy Mater.* **2015**, *5*, 1501063.
[17] N. Qiu, H. Zhang, X. Wan, C. Li, X. Ke, H. Feng, B. Kan, H. Zhang, Q. Zhang, Y. Lu, Y. Chen, *Adv. Mater.* **2017**, *29*, 1604964.
[18] H. Zhang, Y. Liu, Y. Sun, M. Li, W. Ni, Q. Zhang, X. Wan, Y. Chen, *Sci. China: Chem.* **2017**, *60*, 1.
[19] F. Liu, Z. Zhou, C. Zhang, T. Vergote, H. Fan, F. Liu, X. Zhu, *J. Am. Chem. Soc.* **2016**, *138*, 15523.
[20] B. Kan, J. Zhang, F. Liu, X. Wan, C. Li, X. Ke, Y. Wang, H. Feng, Y. Zhang, G. Long, R. H. Friend, A. A. Bakulin, Y. Chen, *Adv. Mater.* **2018**, *30*, 1704904.
[21] F. Liu, T. Hou, X. Xu, L. Sun, J. Zhou, X. Zhao, S. Zhang, *Macromol. Rapid Commun.* **2017**, *39*, 170555.
[22] Y. Lin, J. Wang, Z. G. Zhang, H. Bai, Y. Li, D. Zhu, X. Zhan, *Adv. Mater.* **2015**, *27*, 1170.
[23] Y. Lin, Q. He, F. Zhao, L. Huo, J. Mai, X. Lu, C.-J. Su, T. Li, J. Wang, J. Zhu, Y. Sun, C. Wang, X. Zhan, *J. Am. Chem. Soc.* **2016**, *138*, 2973.
[24] Y. Lin, F. Zhao, Q. He, L. Huo, Y. Wu, T. C. Parker, W. Ma, Y. Sun, C. Wang, D. Zhu, A. J. Heeger, S. R. Marder, X. Zhan, *J. Am. Chem. Soc.* **2016**, *138*, 4955.
[25] Y. Yang, Z.-G. Zhang, H. Bin, S. Chen, L. Gao, L. Xue, C. Yang, Y. Li, *J. Am. Chem. Soc.* **2016**, *138*, 15011.
[26] H. Yao, Y. Chen, Y. Qin, R. Yu, Y. Cui, B. Yang, S. Li, K. Zhang, J. Hou, *Adv. Mater.* **2016**, *28*, 8283.
[27] S. Dai, F. Zhao, Q. Zhang, T.-K. Lau, T. Li, K. Liu, Q. Ling, C. Wang, X. Lu, W. You, X. Zhan, *J. Am. Chem. Soc.* **2017**, *139*, 1336.
[28] S. Xu, Z. Zhou, W. Liu, Z. Zhang, F. Liu, H. Yan, X. Zhu, *Adv. Mater.* **2017**, *29*, 1704510.
[29] S. Li, L. Ye, W. Zhao, S. Zhang, S. Mukherjee, H. Ade, J. Hou, *Adv. Mater.* **2016**, *28*, 9423.
[30] S. Li, L. Ye, W. Zhao, S. Zhang, H. Ade, J. Hou, *Adv. Energy Mater.* **2017**, *7*, 1700183.
[31] H. Feng, N. Qiu, X. Wang, Y. Wang, B. Kan, X. Wan, M. Zhang, A. Xia, C. Li, F. Liu, Y. Chen, *Chem. Mater.* **2017**, *29*, 7908.
[32] S. Li, L. Ye, W. Zhao, X. Liu, J. Zhu, H. Ade, J. Hou, *Adv. Mater.* **2017**, *29*, 1704051.
[33] C. Duan, K. Zhang, C. Zhong, F. Huang, Y. Cao, *Chem. Soc. Rev.* **2013**, *42*, 9071.
[34] M. T. Dang, J. D. Wuest, *Chem. Soc. Rev.* **2013**, *42*, 9105.

[35] Y. Huang, E. J. Kramer, A. J. Heeger, G. C. Bazan, *Chem. Rev.* **2014**, *114*, 7006.
[36] D. Baran, R. S. Ashraf, D. A. Hanifi, M. Abdelsamie, N. Gasparini, J. A. Rohr, S. Holliday, A. Wadsworth, S. Lockett, M. Neophytou, C. J. M. Emmott, J. Nelson, C. J. Brabec, A. Amassian, A. Salleo, T. Kirchartz, J. R. Durrant, I. McCulloch, *Nat. Mater.* **2017**, *16*, 363.
[37] Q. An, F. Zhang, J. Zhang, W. Tang, Z. Deng, B. Hu, *Energy Environ. Sci.* **2016**, *9*, 281.
[38] L. Nian, K. Gao, F. Liu, Y. Kan, X. Jiang, L. Liu, Z. Xie, X. Peng, T. P. Russell, Y. Ma, *Adv. Mater.* **2016**, *28*, 8184.
[39] W. Zhao, S. Li, S. Zhang, X. Liu, J. Hou, *Adv. Mater.* **2017**, *29*, 1604059.
[40] Z. Xiao, X. Jia, L. Ding, *Sci. Bull.* **2017**, *62*, 1562.
[41] L. Lu, M. A. Kelly, W. You, L. Yu, *Nat. Photonics* **2015**, *9*, 491.
[42] T. Liu, L. Huo, X. Sun, B. Fan, Y. Cai, T. Kim, J. Kim, H. Choi, Y. Sun, *Adv. Energy Mater.* **2016**, *6*, 1502109.
[43] H. Fu, Z. Wang, Y. Sun, *Sol. RRL* **2018**, *2*, 1700158.
[44] N. Felekidis, E. Wang, M. Kemerink, *Energy Environ. Sci.* **2016**, *9*, 257.
[45] J. Zhang, C. Yan, W. Wang, Y. Xiao, X. Lu, S. Barlow, T. C. Parker, X. Zhan, S. R. Marder, *Chem. Mater.* **2018**, *30*, 309.
[46] H. Fu, Z. Wang, Y. Sun, *Adv. Mater.* **2017**, *29*, 1700158.
[47] T. Liu, Y. Guo, Y. Yi, L. Huo, X. Xue, X. Sun, H. Fu, W. Xiong, D. Meng, Z. Wang, F. Liu, T. P. Russell, Y. Sun, *Adv. Mater.* **2016**, *28*, 10008.
[48] R. Yu, S. Zhang, H. Yao, B. Guo, S. Li, H. Zhang, M. Zhang, J. Hou, *Adv. Mater.* **2017**, *29*, 1700437.
[49] W. G. Jiang, R. N. Yu, Z. Y. Liu, R. X. Peng, D. B. Mi, L. Hong, Q. Wei, J. H. Hou, Y. B. Kuang, Z. Y. Ge, *Adv. Mater.* **2018**, *30*, 1703005.
[50] T. M. Clarke, J. R. Durrant, *Chem. Rev.* **2010**, *110*, 6736.
[51] Z.-G. Zhang, B. Qi, Z. Jin, D. Chi, Z. Qi, Y. Li, J. Wang, *Energy Environ. Sci.* **2014**, *7*, 1966.
[52] C. J. Brabec, S. Gowrisanker, J. J. Halls, D. Laird, S. Jia, S. P. Williams, *Adv. Mater.* **2010**, *22*, 3839.
[53] P. W. Blom, V. D. Mihailetchi, L. J. A. Koster, D. E. Markov, *Adv. Mater.* **2007**, *19*, 1551.
[54] C. M. Proctor, M. Kuik, T.-Q. Nguyen, *Prog. Polym. Sci.* **2013**, *38*, 1941.
[55] O. Ostroverkhova, *Chem. Rev.* **2016**, *116*, 13279.
[56] F. Liu, Y. Gu, X. Shen, S. Ferdous, H.-W. Wang, T. P. Russell, *Prog. Polym. Sci.* **2013**, *38*, 1990.
[57] D.-M. Smilgies, *J. Appl. Crystallogr.* **2009**, *42*, 1030.
[58] J. Rivnay, S. C. Mannsfeld, C. E. Miller, A. Salleo, M. F. Toney, *Chem. Rev.* **2012**, *112*, 5488.
[59] P. Müller-Buschbaum, *Adv. Mater.* **2014**, *26*, 7692.